SATELLITE & MESOMETEOROLOGY
RESEARCH PROJECT

Department of the Geophysical Sciences
The University of Chicago

MISO-SCALE STRUCTURE OF DOWNBURSTS DEPICTED BY DOPPLER RADAR

by T. Theodore Fujita

Supplement to
DOWNBURSTS AND MICROBURSTS -- AN AVIATION HAZARD
Preprint Volume: 19th Conference on Radar Meteorology, AMS, pp 94-101
April 15-18, 1980; Miami Beach, Florida

SMRP Research Paper 181

April 1980

MISO-SCALE STRUCTURE OF DOWNBURSTS

DEPICTED BY DOPPLER RADARS

by

T. Theodore Fujita

SUPPLEMENT TO

DOWNBURSTS AND MICROBURSTS -- AN AVIATION HAZARD

Preprint Volume: 19th Conference on Radar Meteorology, AMS, pp 94-101
April 15-18, 1980; Miami Beach, Florida

Abstract

Two microbursts, depicted by the NIMROD (Northern Illinois Meteorological Research On Downbursts) network were analyzed in detail.

The first microburst, identified as the "Yorkville Microburst", descended into the warm-sector boundary layer resulting in 4.5 °C cooling and 21.2 m/sec peak wind on the ground. Doppler velocities by the Yorkville radar revealed that the outburst winds were about 1000 m across with its maximum wind of 32 m/sec only 20 to 30 m above the ground.

The second microburst, called the "O'Hare Microburst", occurred 17 km west of the O'Hare International Airport with its 23 m/sec outburst winds at 200 to 250 m above the ground. This microburst descended into the cold boundary layer 30 km behind a well-defined gust front which swept across the airport area. The downflow speed of the Yorkville Microburst was 3 m/sec at 100 m and 11 m/sec at 500 m AGL. The O'Hare Microburst was accompanied by 1.5 m/sec downflow at 100 m and 5.5 m/sec at 500 m AGL. The active life of both microbursts was less than 15 minutes.

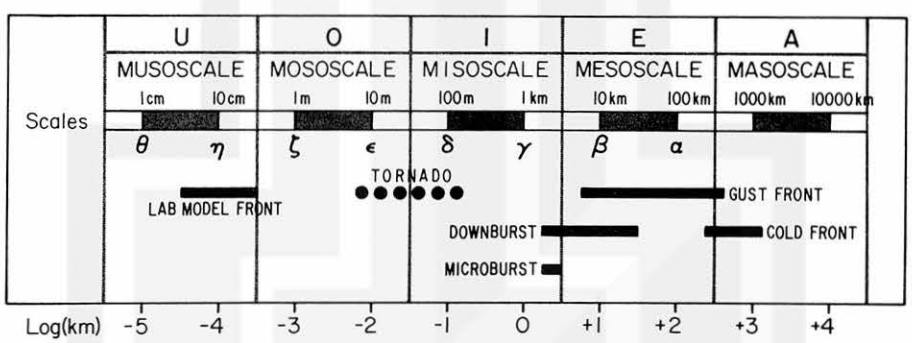

Figure 1. Five scales of atmospheric motion proposed by Fujita (1979). Horizontal dimensions of downburst extend from misoscale to mesoscale. Misoscale downburst is called microburst.

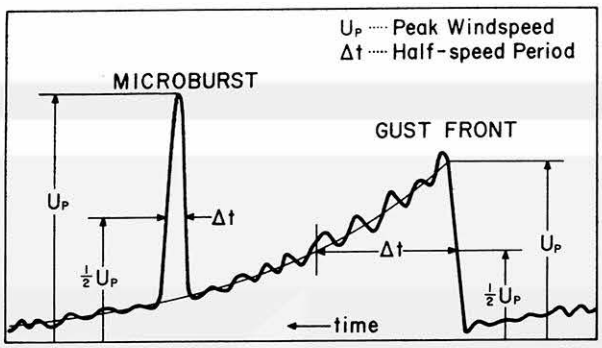

Figure 2. Definition of the half-speed period applicable to downburst and gust front. Half-speed periods of microbursts are only up to several minutes.

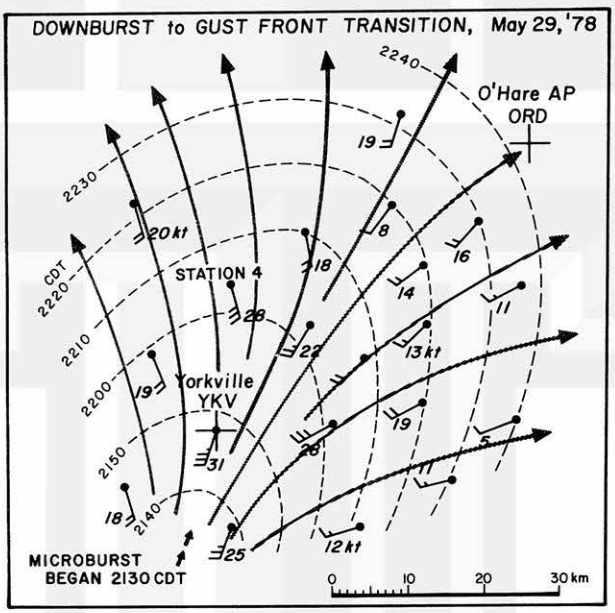

Figure 3. Peak windspeeds and isochrones of high winds which swept across the NIMROD network on May 29, 1978. Winds were measured by the PAM stations as outflows of downbursts gradually turned into an expanding gust front.

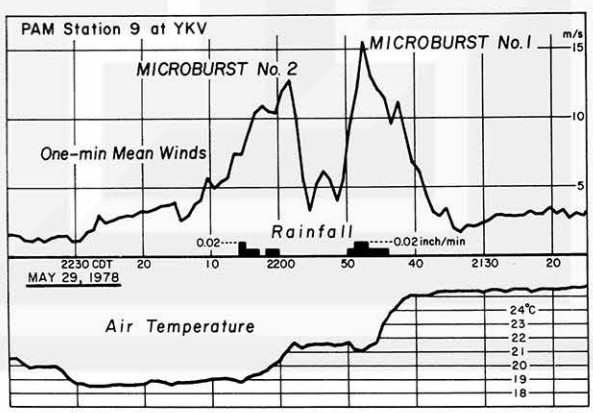

Figure 4. Windspeed and temperature measured by PAM 7 at the YKV Doppler radar site. Microburst No.1 descended inside the warm air while, No.2, inside the cold boundary layer created by No.1.

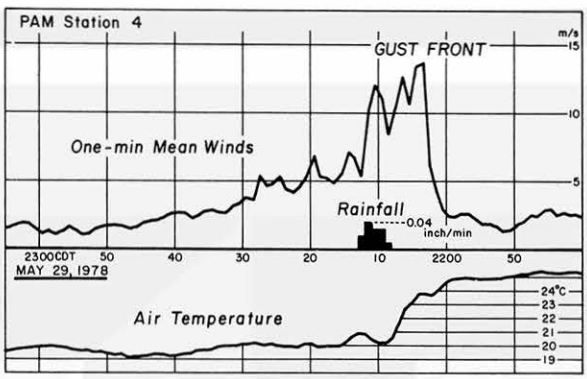

Figure 5. Windspeeds of the gust front as it passed over PAM station No. 4.

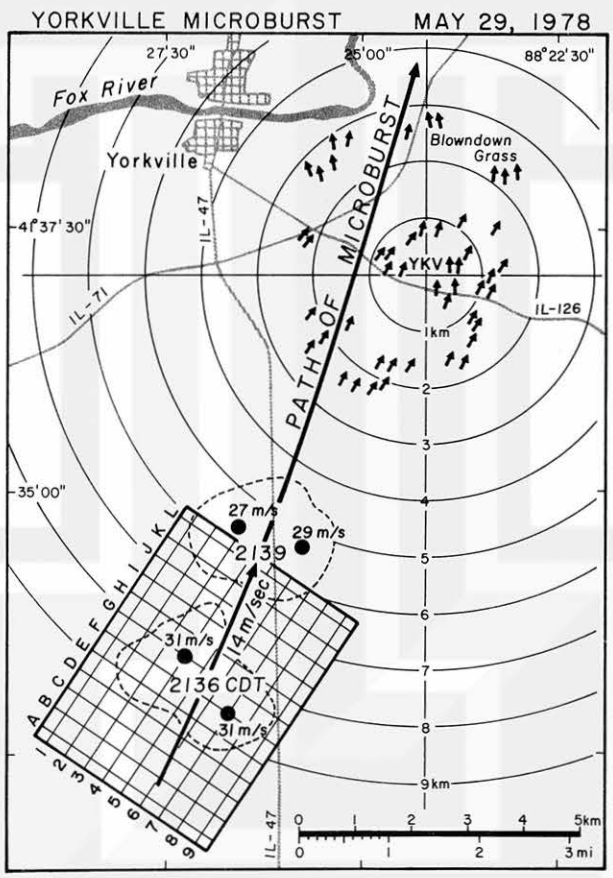

Figure 6. Path of a microburst depicted by the YKV Doppler radar on May 29, 1978. A rectangular area gridded with lines 1 through 9 and letters A through L was placed over the microburst at 2136 CDT.

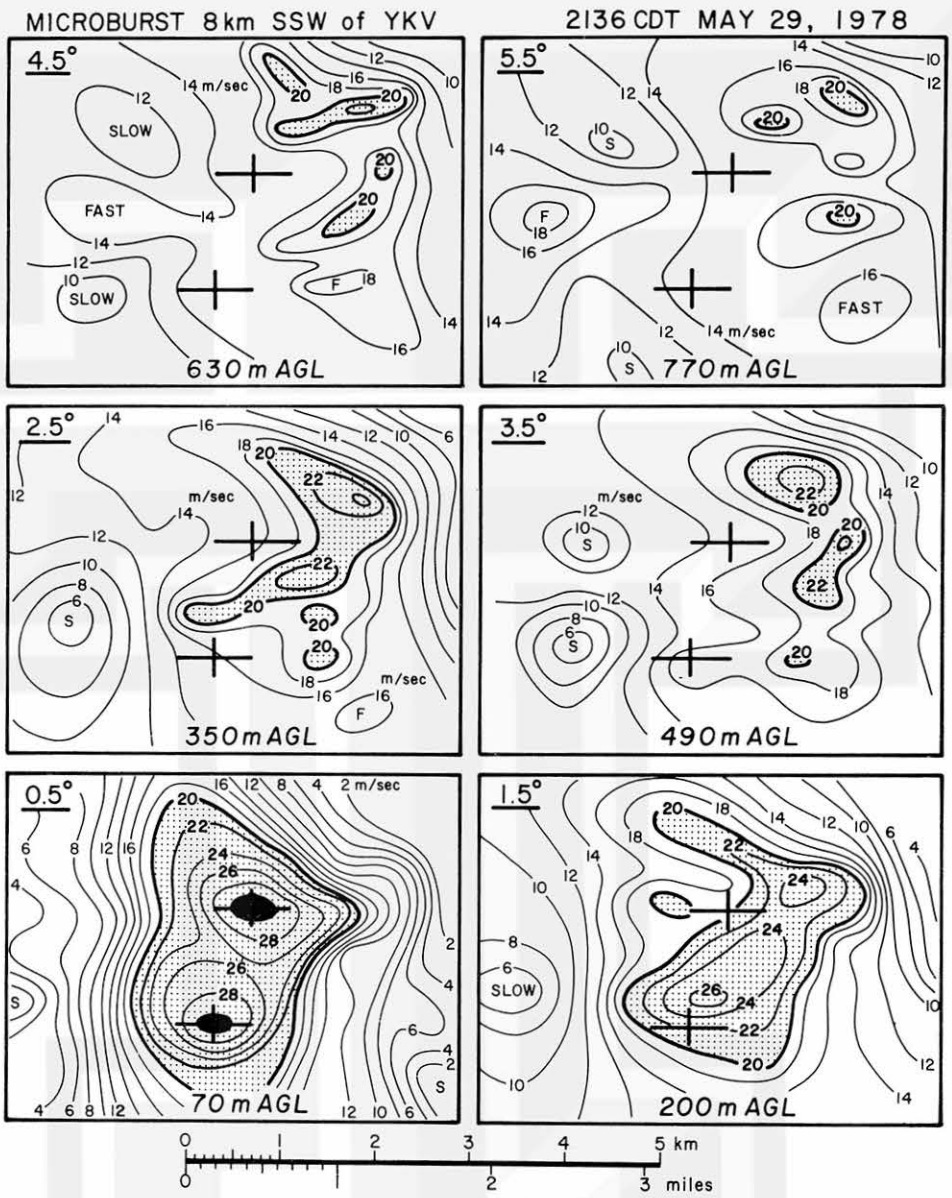

Figure 7. Patterns of radial velocities toward the YKV radar obtained by changing the elevation angles of the beam from 0.5 to 5.5 degrees at one-degree intervals. The AGL heights of the beam near the grid center increased from 70 to 770m.

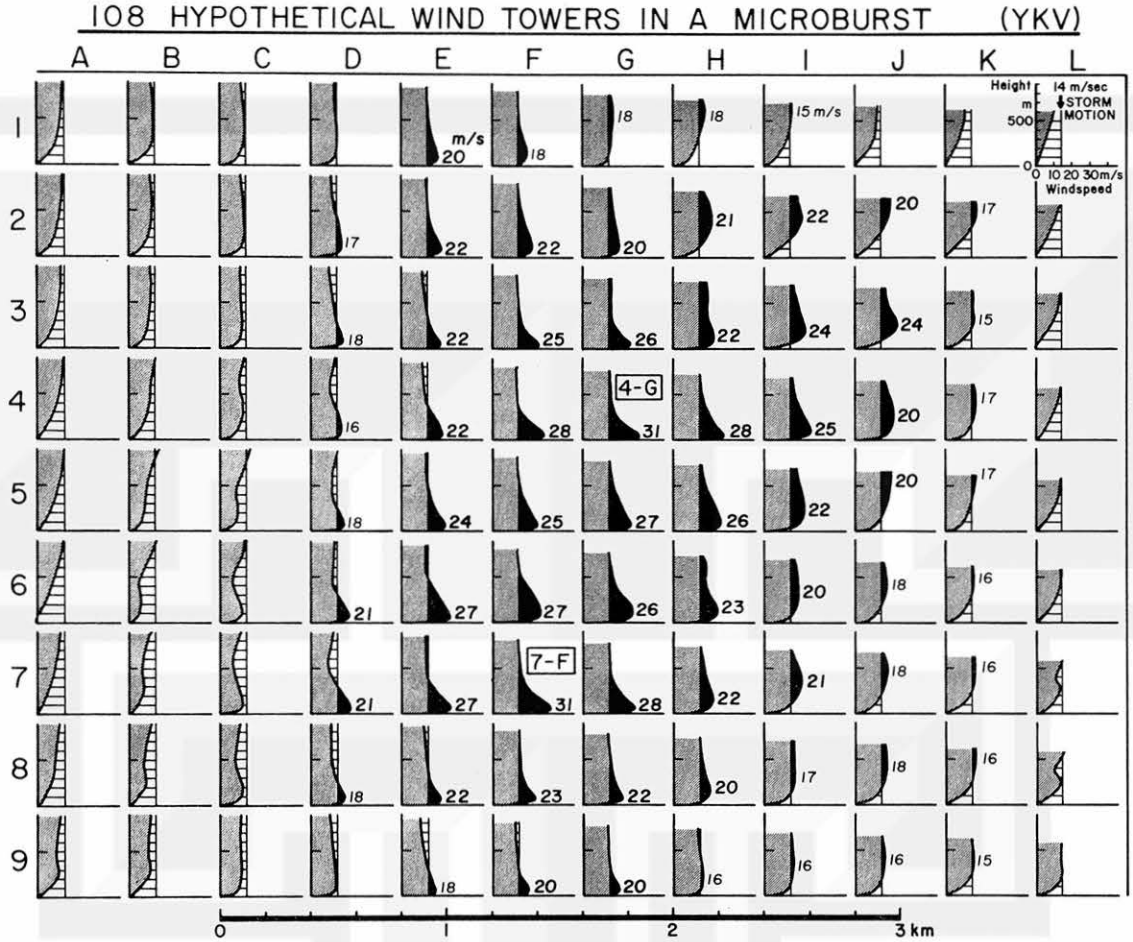

Figure 8. Vertical distribution of radial winds at the 108 grid points in the rectangular area in Figure 6. Two centers of the maximum winds in Figure 7 are located at Lines 4 and G (4-G) and at lines 7 and F (7-F). Speeds in excess of the storm motion of 14 m/sec are painted and those less than the storm motion are shaded.

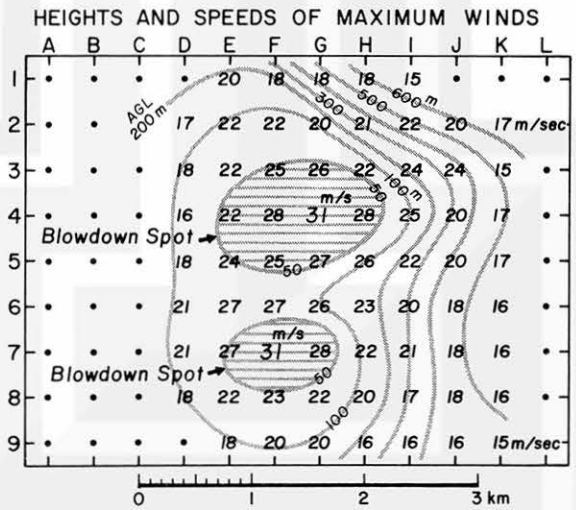

Figure 9. Heights and speeds of the maximum wind along the local vertical at each grid point. Heights are contoured and speeds are numbered. This figure reveals that the faster the maximum windspeeds the lower their heights. Blowdown spots, where trees and vegetation are likely to be damaged, are only about one kilometer across.

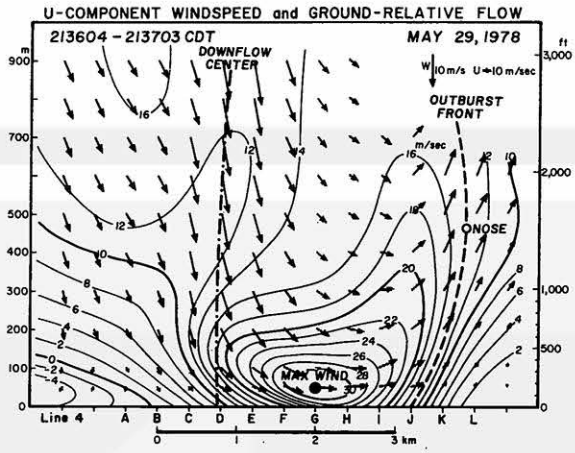

Figure 10. Isotachs of horizontal windspeeds across line 4. The height of the maximum wind is estimated to be 50 m or lower. Arrows are ground-relative velocities in the plane which is stretched vertically.

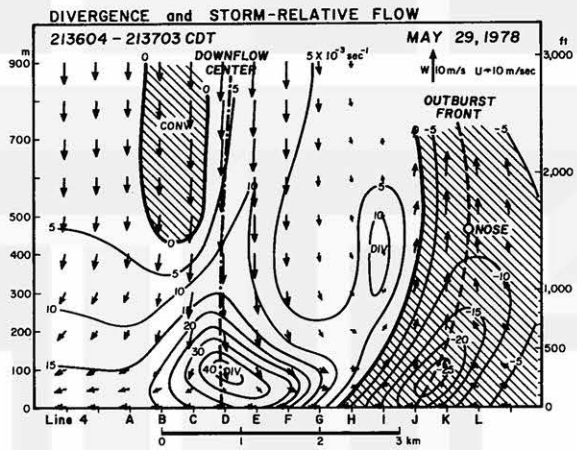

Figure 11. Divergence in the vertical plane of Figure 10. The maximum divergence located below 100m AGL is about 0.05 per second. Arrows denote storm-relative velocities.

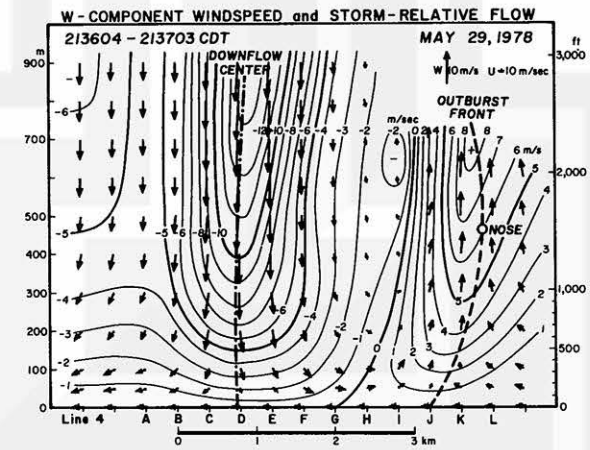

Figure 12. Vertical velocities computed from the divergence pattern in Figure 13. It is seen that the downflow speed at 1000m AGL is about 14m/sec. The 75% of the downflow speed at 1000m is seen at 500m and 50% at 250m AGL.

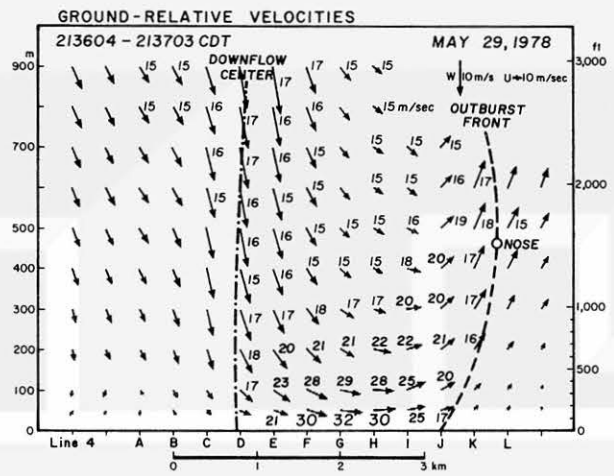

Figure 13. The total windspeeds in the vertical plane. 15m/sec or higher speeds are numbered. It should be noted that the highest speed of 32m/sec at 4-G is located at about 50m AGL and 1200m ahead of the downflow center.

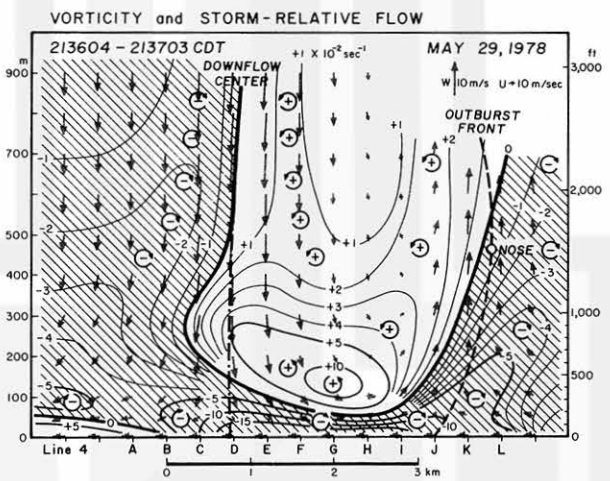

Figure 14. Distribution of vorticity in the vertical plane. A pair of large positive and negative vorticities is created on both sides of the maximum horizontal wind just above the ground. Another pair of weak vorticities is transported downward on both sides of the downflow center.

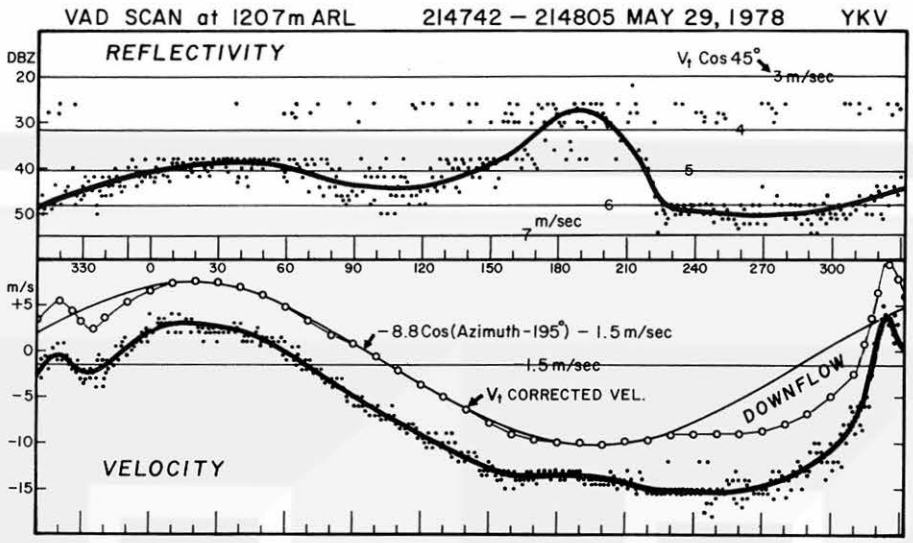

Figure 15. Reflectivity and velocity values obtained with a 45-deg elevation angle during the Yorkville microburst. This display shows the data of the 8th gate extending between the 1,632 and 1,782 m range. The height at the median range is 1,207 m above the radar level (ARL). The deficit of the velocity from the best-fit sinusoidal curve is assumed to be downflow speed.

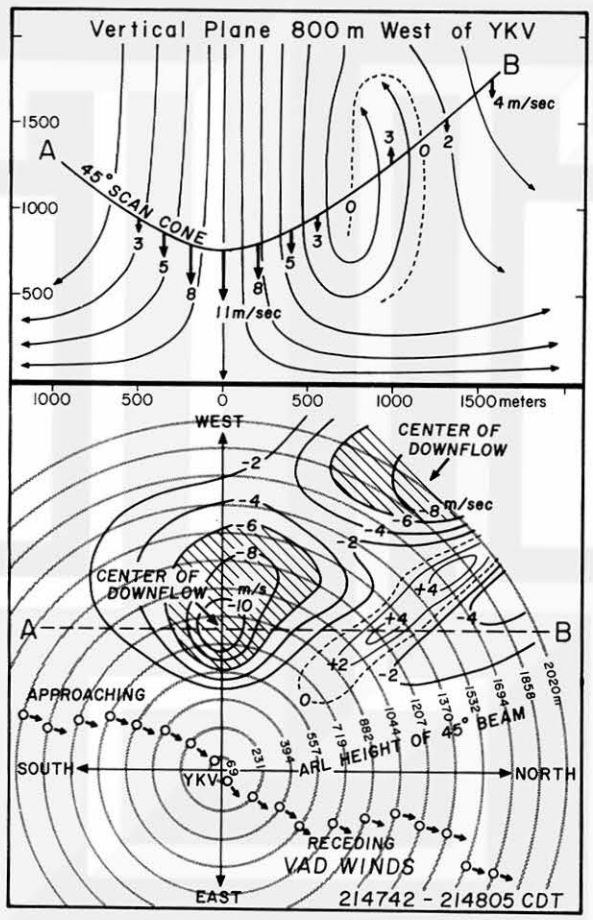

Figure 16. Distribution of the downflow speeds on the 45-deg conical surface (below). Vertical velocities in the vertical plane through the center of the downflow, 800 m to the west of the YKV radar. The hyperbola, A-B is the intersection between the scan cone and the vertical plane (above).

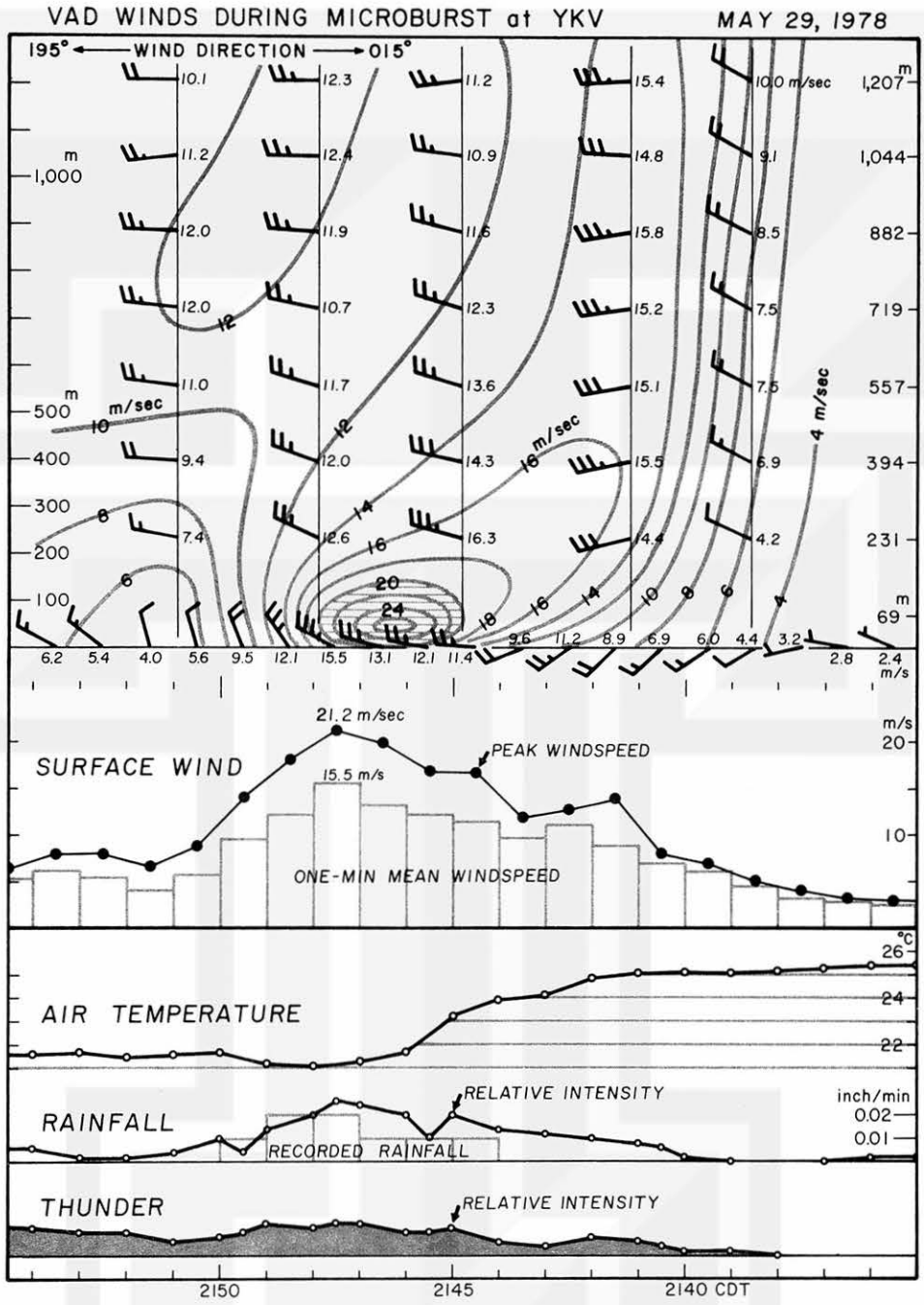

Figure 17. Time cross section of VAD winds obtained by the YKV radar during the microburst. It should be noted that the PAM winds measured at 7-m AGL reached the peak at 2148 CDT, while the maximum speed at 50 m occurred one to two minutes earlier, and that at 300 m, 5-min earlier.

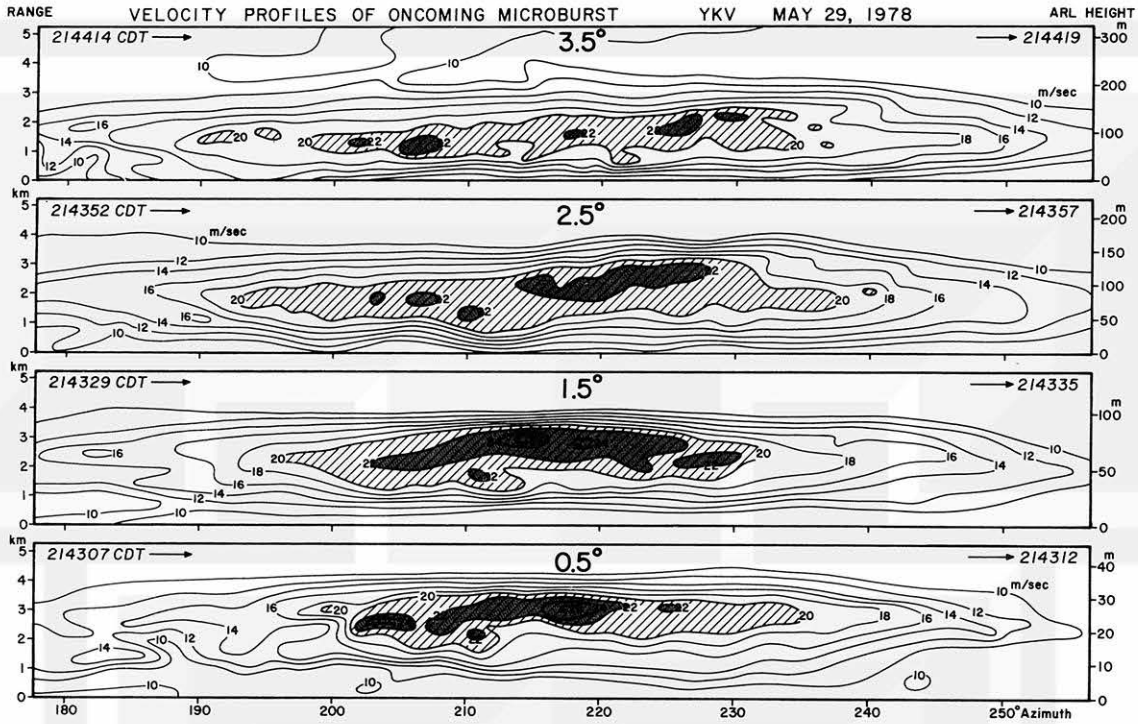

Figure 18. Velocity profiles of the oncoming microburst in Figure 17 when the maximum winds were about 3 km to the southwest of the radar. Scales on the left side denote the range from YKV and those on the right side, the ARL height of the radar beam.

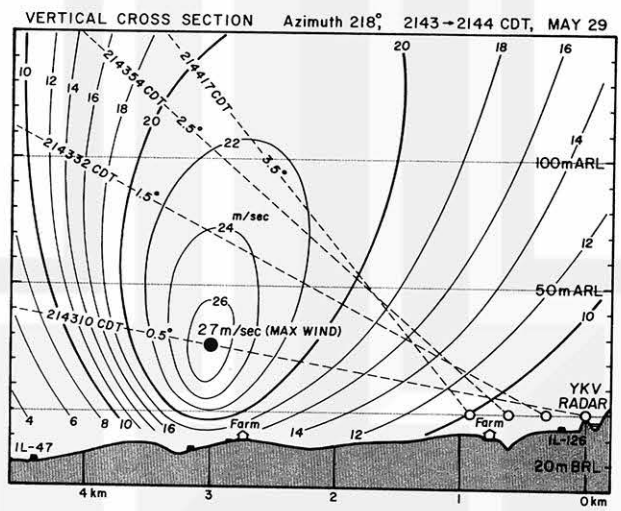

Figure 19. A cross section of Doppler velocity within the vertical plane of 218-deg azimuth. In constructing this diagram, the YKV radar was moved toward the microburst at the approaching speed of the system. The height of the maximum wind turned out to be very low, only 20 to 60 m ARL.

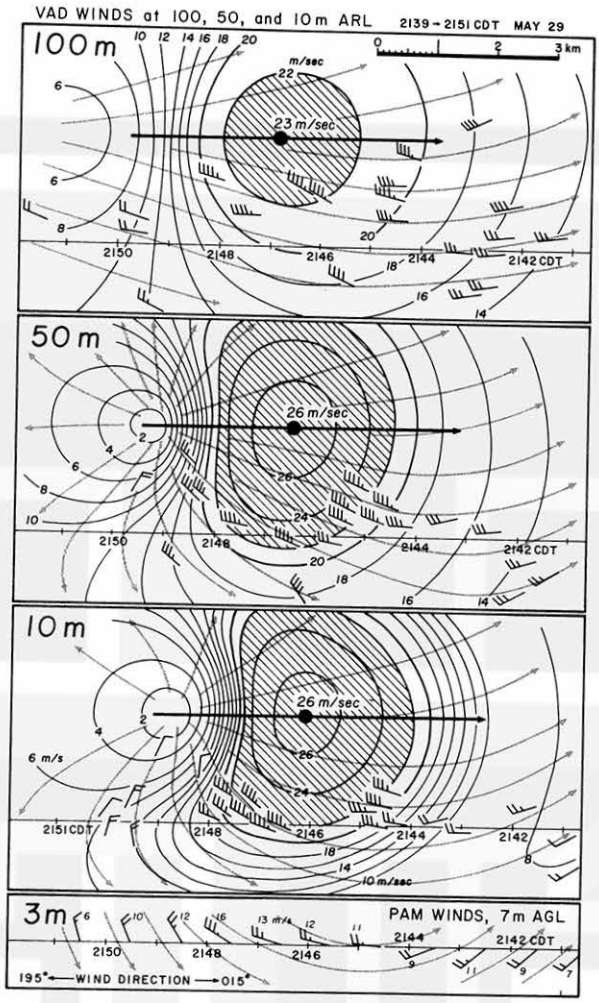

Figure 20. VAD winds at three levels at 10, 50, and 100 m ARL. In constructing these time-adjusted maps, the YKV radar was moved at 14 m/sec toward the 195-deg azimuth and each wind vector from VAD scans was plotted at its azimuth and range. Wind directions are relative to the 195 (left) to 015-deg azimuth. The radar-relative flows reveal the existence of a significant divergence at 10 to 50 m ARL where the maximum winds of the outburst was taking place.

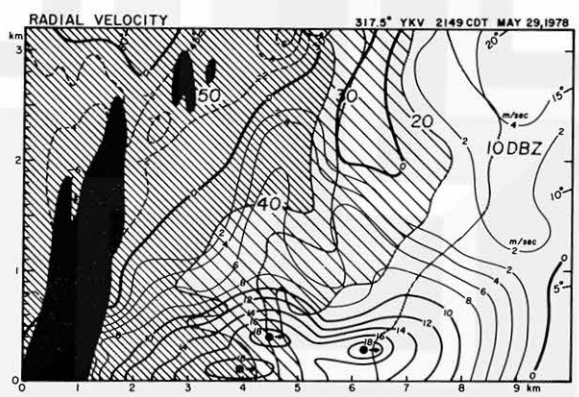

Figure 21. RHI cross section of reflectivity and velocity through 200 to 300 m to the southwest of the downflow in Figure 16. Terminal velocities computed from reflectivity were subtracted. The scan time was between 214850 CDT and 214902, during which the beam was brought down from the zenith to 1.3 degrees. Three centers of the maximum windspeed suggest the existence of successive outflows which are turning into the gust frontin Figure 3.

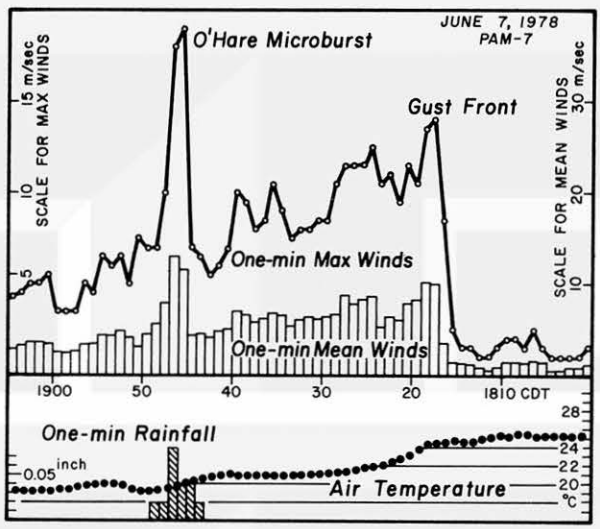

Figure 22. Windspeed, temperature, and rainfall recorded by the PAM Station No. 7 during the passage of a gust front and a microburst on June 7, 1978. The microburst identified as "O'Hare Microburst" descended inside the cold sector accompanied by a 38 kt peak wind and 4.8 inches per hour rainfall.

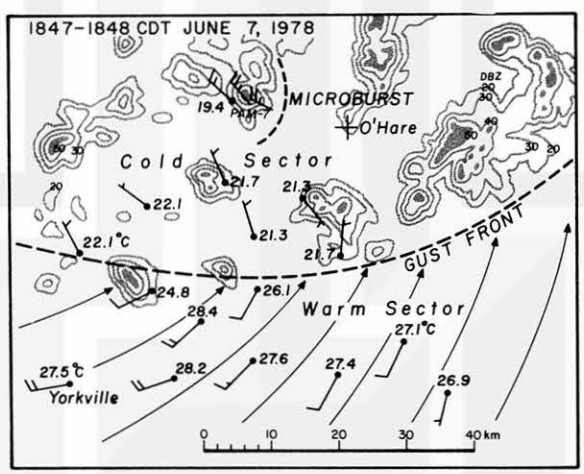

Figure 23. Mesosynoptic map of the gust front and the microburst in Figure 22. The microburst was associated with a small echo with 50 DBZ reflectivity.

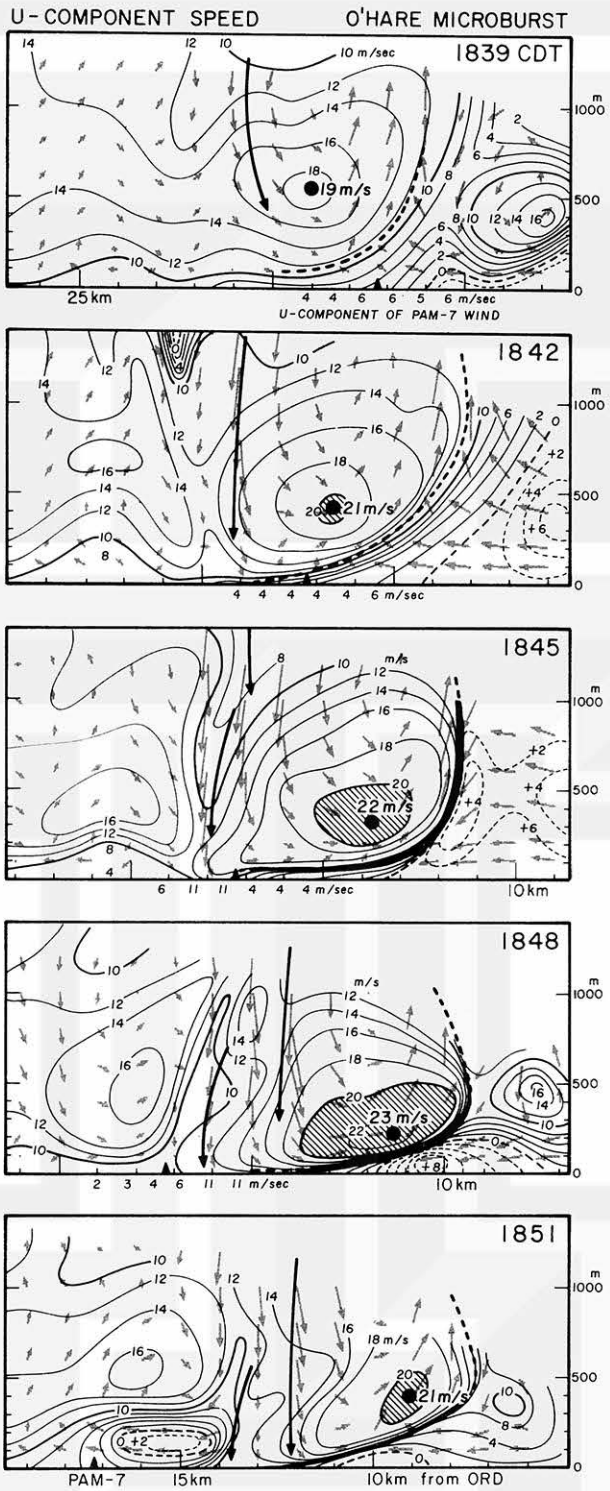

Figure 24. Vertical cross-section of the U-component windspeeds measureed by the O'Hare Doppler radar. Speeds in excess of 20 m/sec are hatched along with the location of the maximum wind shown with a painted circle. The U-component speeds of PAM-7 winds were indicated at the bottom by using the storm movement at 12 m/sec. Arrows show storm-relative winds within the vertical plane.

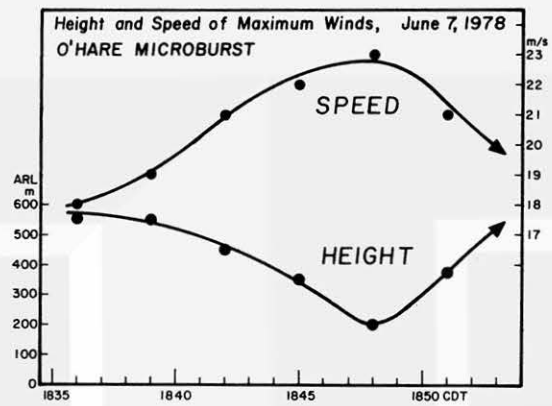

Figure 25. Time variation of the height and speed of the maximum wind of O"Hare microburst. The maximum windspeed increased as its height descended to about 200-m ARL.

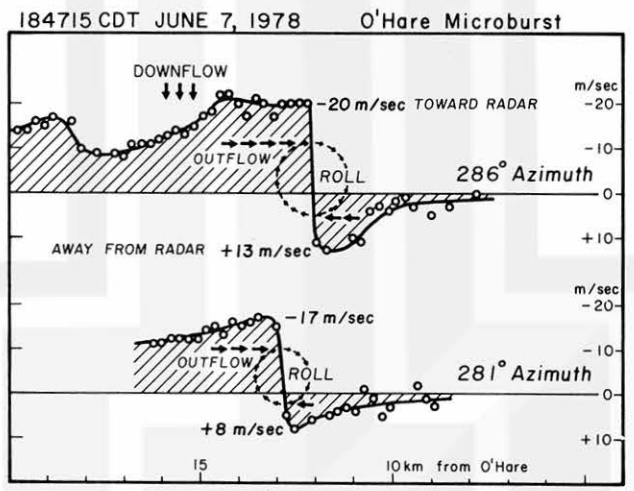

Figure 26. Gate-by-gate variation of radial velocities measured by the O'Hare Doppler radar. The height of the 0.5-deg beam is 90 m ARL at 10 km and 130 m at 15 km range from O'Hare. The radial velocity changed from -20 m/sec to +13 m/sec within one to two gates. Gate length was 230 m.

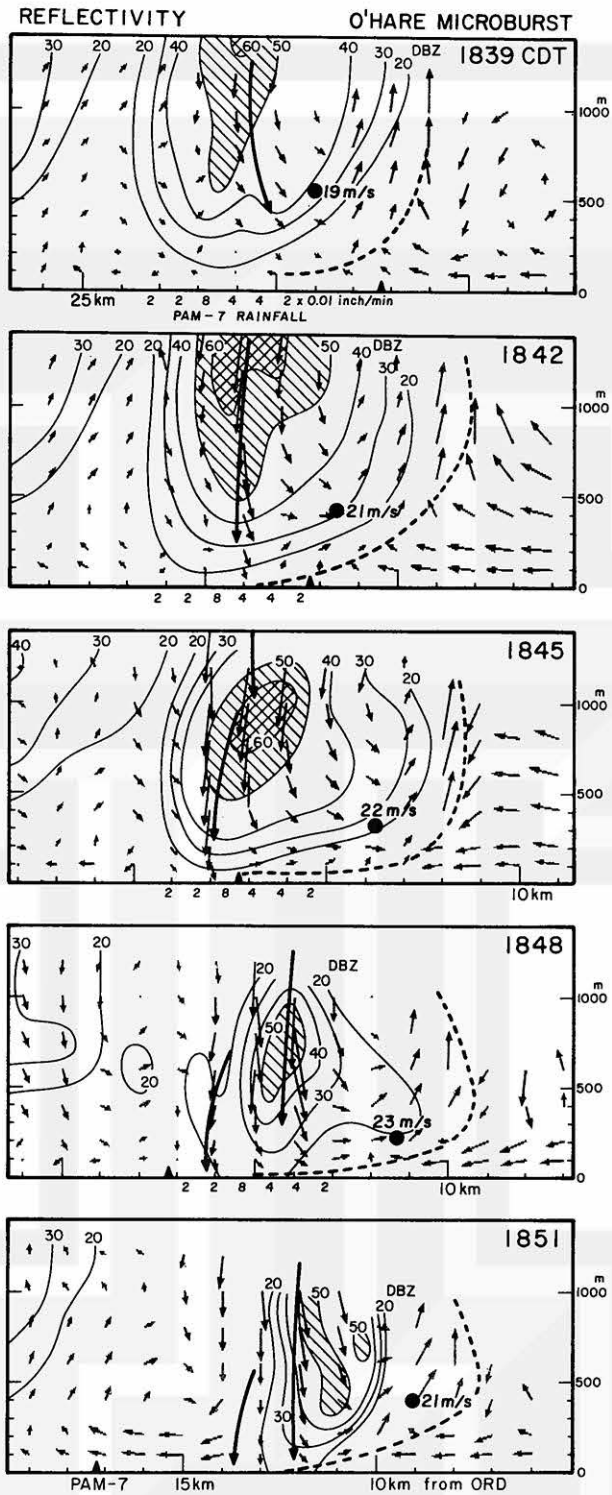

Figure 27. Vertical cross section of reflectivity within the vertical plane including O'Hare Doppler radar and PAM 7. DBZ values at the location of the maximum outflow wind decreased from 37 DBZ at 1839 to 19 DBZ at 1848 CDT, revealing that the high winds dashed out of high-reflectivity regions. The maximum wind at 1851 CDT was located one kilometer ahead of the 20 DBZ echo boundary.

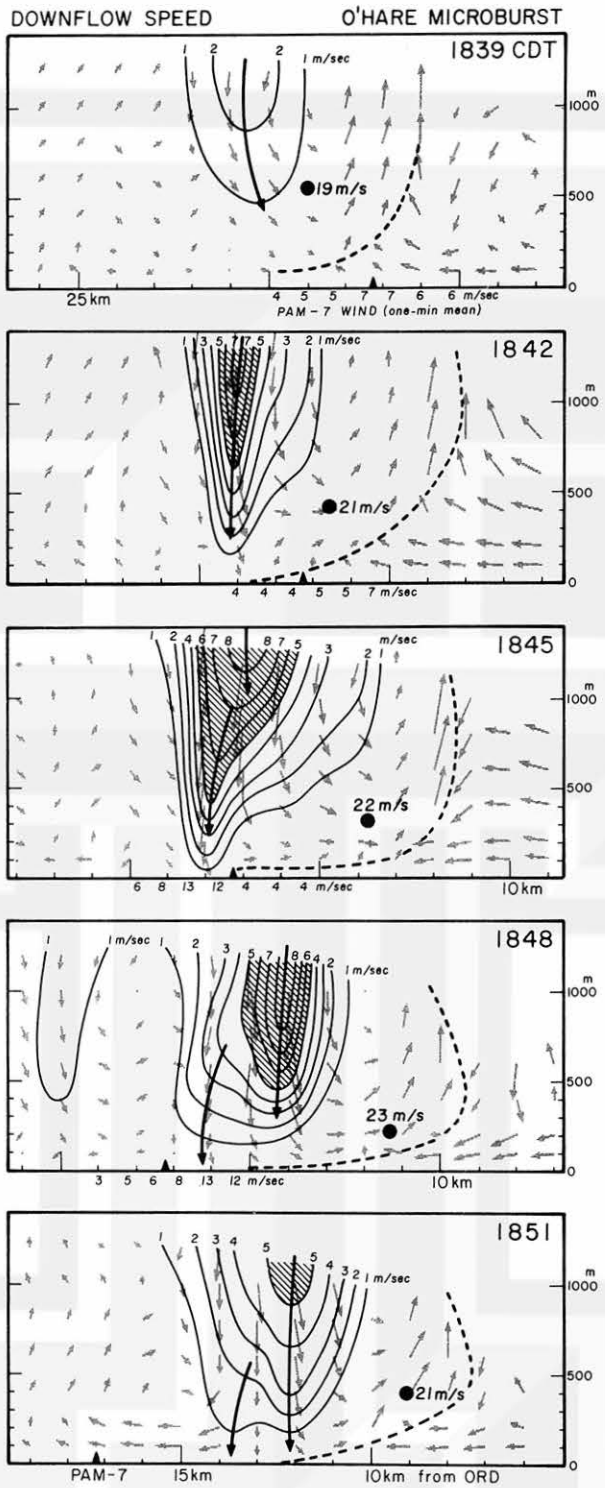

Figure 28. Vertical cross section of the downflow speed of O'Hare microburst. The horizontal winds measured by PAM 7 remained less than 7 m/sec while the maximum wind in excess of 22 m/sec passed over the station. PAM-7 winds reached the peak when the downflow descended, bringing the horizontal momentum down to the ground. Note that the maximum downflow and outflow winds are separated by 2 to 3 km horizontally.

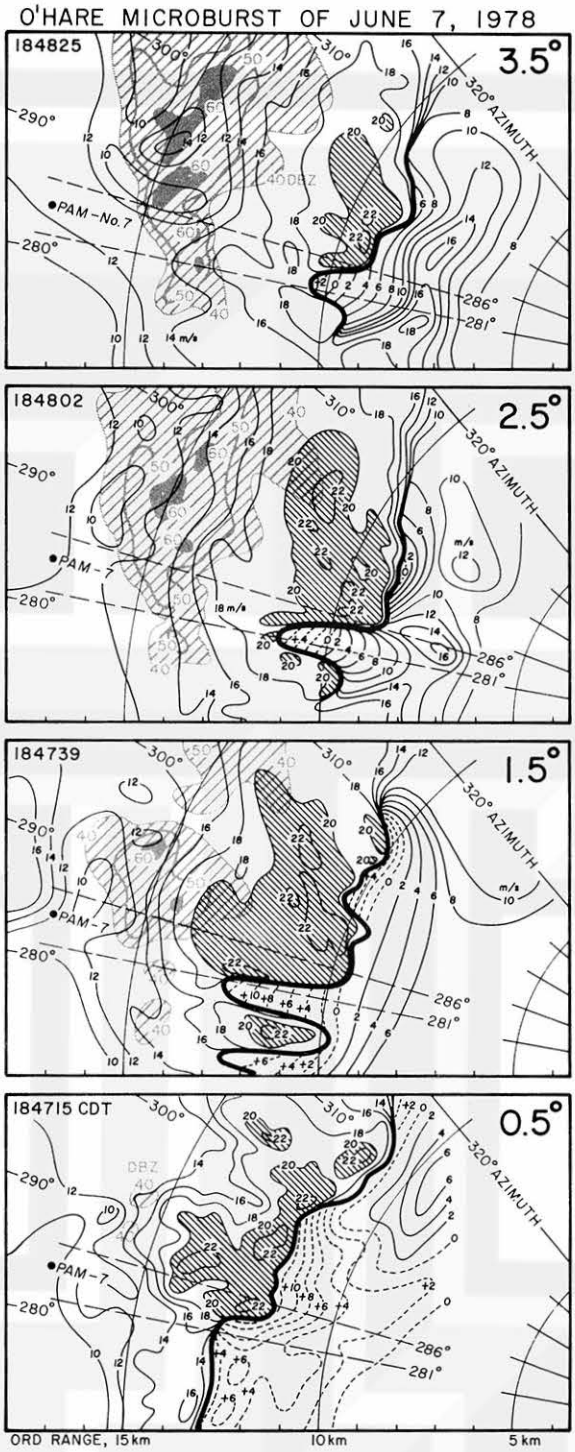

Figure 29. Distribution of radial velocities corresponding to four different elevation angles, 0.5, 1.5, 2.5, and 3.5 degrees. The zone of tight velocity gradient shifted toward O'Hare showing the existence of a sloped overruning outflow. The slope was estimated to be 160 m per 2000 m or 8/100, rising toward O'Hare. The wind shear across this slope was -22 m/sec(above) to +12 m/sec (below the surface).

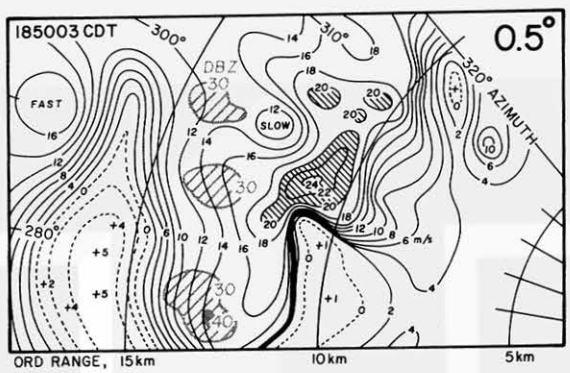

Figure 30. Radial velocity of O'Hare microburst obtained with 0.5-deg elevation angle three minutes after the scan time of Figure 29. Within a few minutes, the tight velocity gradient was gone, suggesting that the wind field near the surface changes very rapidly.

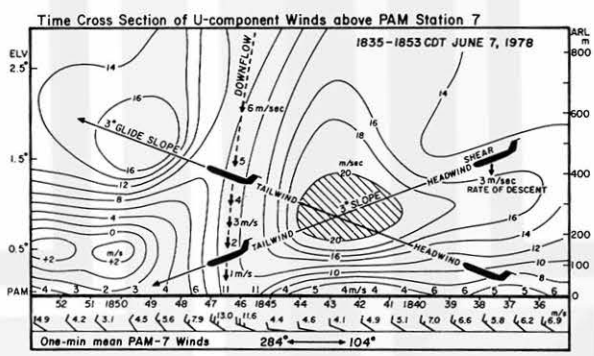

Figure 31. Hypothetical penetration through the maximum-wind core along 3-deg slopes. The headwind shear (headwind increase with time) is experienced during the approach to the core, while the tailwind shear (headwind decrease or tailwind increase with time) is encountered while flying away from the core. A strong tailwind shear results in a loss of airspeed which endangers both landing and takeoff operations. It should be noted that PAM 7 failed to measure high winds until three minutes after the passage of the maximum wind less than 300 m above the station.

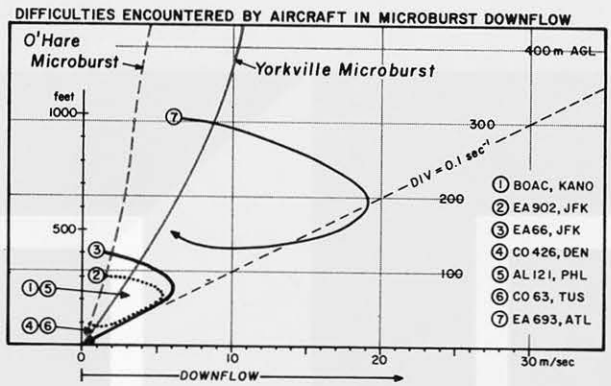

Figure 32. Vertical distribution of downflow speeds encountered by seven aircraft during either liftoff or landing stage. The magnitude of the near-ground divergence was up to 0.1 per sec. Yorkville microburst (warm sector) and O'Hare microburst (cold sector) were characterized by 0.04 and 0.02 per sec divergence near the ground, respectively.

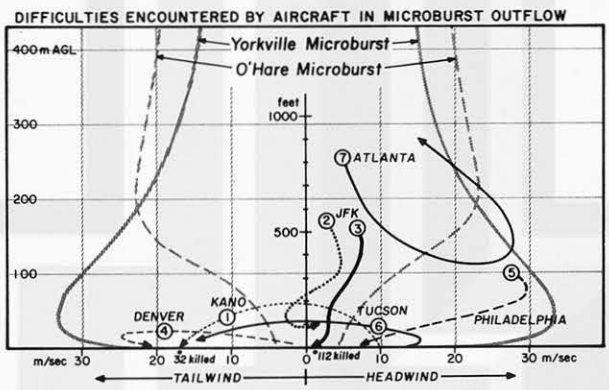

Figure 33. Vertical distribution of outflow speeds encountered by the seven aircraft in Figure 32. Since outflow winds induced bymicroburst could be either headwind or tailwind, depending upon the direction of penetration, mirror-image profiles of Yorkville and O'Hare microbursts were included in this figure. Practically all accident cases occurred below 500 ft above the ground where outflow windspeeds are the strongest.